Biophysical Chemistry 271 (2021) 106563

Contents lists available at ScienceDirect

Biophysical Chemistry

journal homepage: www.elsevier.com/locate/biophyschem

Characterisation of the structural, dynamic and aggregation properties of the W64R amyloidogenic variant of human lysozyme

Nicola Vettore [a], Joël Moray [a], Alain Brans [a], Raphaël Herman [a], Paulette Charlier [a], Janet R. Kumita [b,1], Frédéric Kerff [a], Christopher M. Dobson [b], Mireille Dumoulin [a,*]

[a] Centre for Protein Engineering, InBioS, Department of Life Sciences, University of Liège, (Sart-Tilman) 4000 Liège, Belgium
[b] Department of Chemistry, University of Cambridge, Lensfield Road, Cambridge CB2 1EW, United Kingdom

ARTICLE INFO

Keywords:
Human lysozyme
Amyloidogenic variants
Protein destabilisation
Fibril formation
Limited proteolysis
Structural cooperativity

ABSTRACT

The accumulation in vital organs of amyloid fibrils made of mutational variants of lysozyme (HuL) is associated with a human systemic amyloid disease. The detailed comparison of the *in vitro* properties of the I56T and D67H amyloidogenic variants to those of the T70N non-amyloidogenic variant and the wild-type (WT) protein suggested that the deposition of large amounts of aggregated disease-related lysozyme variants is initiated by the formation of transient intermediate species. The ability to populate such intermediates is essentially due to the destabilisation of the protein and the loss of the global structural cooperativity under physiologically relevant conditions. Here, we report the characterisation of a third naturally occurring amyloidogenic lysozyme variant, W64R, in comparison with the I56T and WT proteins. The X-ray crystal structure of the W64R variant at 1.15 Å resolution is very similar to that of the WT protein; a few interactions within the β-domain and at the interface between the α- and β-domains differ, however, from those in the WT protein. Consequently, the W64R mutation destabilizes the protein to an extent that is similar to that observed for the I56T and D67H mutations. The $\Delta G^{\circ}_{NU}(H_2O)$ is reduced by 24 kJ·mol^{-1} and the T_m is about 12 °C lower than that of the WT protein. Under native conditions, the W64R and I56T proteins are readily digested by proteinase K, while the WT protein remains intact. These results suggest that the two variant proteins transiently populate similar partially unfolded states in which proteinase K cleavage sites are accessible to the protease. Moreover, the *in vitro* aggregation properties of the W64R protein are similar to those of the I56T variant. Altogether, these results indicate that the properties of the W64R protein are astonishingly similar to those of the I56T variant. They further corroborate the idea that HuL variants associated with the disease are those whose stability and global structural cooperativity are sufficiently reduced to allow the formation of aggregation prone partially folded intermediates under physiological conditions.

1. Introduction

Human lysozyme (HuL) is a bacteriolytic enzyme present in various tissues and body fluids including the liver, cartilage, saliva, tears and plasma [1,2]. The aggregation of a series of mutational variants of HuL into amyloid fibrils is causative of lysozyme amyloidosis (ALys), a rare autosomal dominant hereditary systemic amyloidosis. The clinical manifestations associated with ALys are broad; they essentially involve the digestive tract, liver, spleen, kidneys, lymph nodes, skin, and lachrymal and salivary glands [1–3]. A cardiac involvement and peripheral neuropathy have also been recently documented [4].

ALys was first identified in 1993 in two unrelated English families by Pepys and co-workers. They discovered that the lysozyme gene of the affected members of each family carried an heterozygous point mutation [5]. In one family, the highly conserved isoleucine at position 56 was mutated to threonine, and the highly conserved aspartic acid at position 67 was mutated to histidine in the other family. It was shown that amyloid fibrils isolated from the tissues of the affected patients contain the full-length lysozyme variant [5]. Since then, several other amyloidogenic variants have been reported that are all located within the β-domain (Fig. 1) [4,6–8]. Two non-amyloidogenic variants have also been reported (*i.e.* T70N and W112R); they are not associated with ALys

* Corresponding author.
E-mail address: mdumoulin@uliege.be (M. Dumoulin).
[1] Present address: Department of Pharmacology, University of Cambridge, Tennis Court Road, Cambridge CB2 1PD, United Kingdom

https://doi.org/10.1016/j.bpc.2021.106563
Received 15 November 2020; Received in revised form 5 February 2021; Accepted 6 February 2021
Available online 13 February 2021

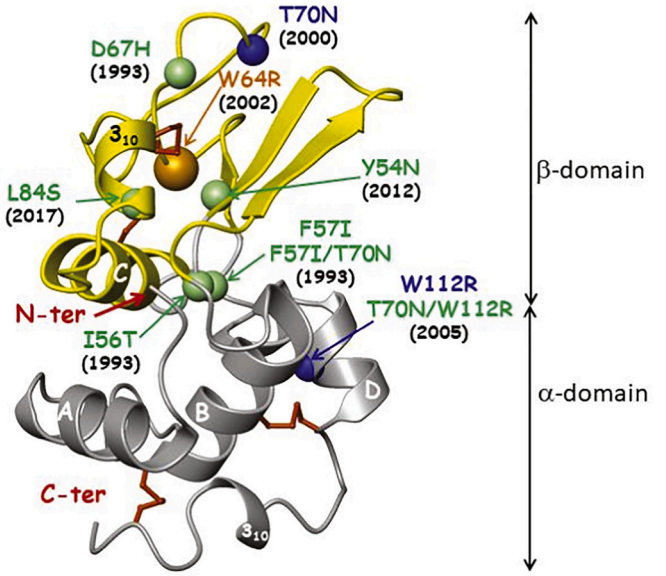

Fig. 1. Structural localisation of the naturally occurring lysozyme variants mapped on the structure of wild-type human lysozyme [11] (PDB code 1LZ1). The four α-helices in the α-domain are labelled A through D. The four disulphide bonds are shown in red. The year of the discovery of each variant is indicated in parenthesis. The W64R mutation is highlighted in orange and the other amyloidogenic mutations are shown in green. The T70N and W112R mutations, shown in blue, are not associated with ALys except when present simultaneously. The regions that are simultaneously and cooperatively unfolded in the intermediate species populated transiently by the I56T and D67H variants are shown in yellow. (For interpretation of the references to colour in this figure legend, the reader is referred to the web version of this article.)

except in individuals carrying both mutations [9,10].

The W64R variant was the third amyloidogenic lysozyme to be reported. It was identified at the genetic level and by immunostaining of the amyloid deposits using an anti-lysozyme antibody [6]. Recently, mass spectrometry-based proteomic analyses of kidney tissues [8] and gastrointestinal tissues [12] from other patients bearing the W64R mutation confirmed that the deposits comprised the W64R lysozyme variant, while no wild-type HuL (WT-HuL) could be detected. Contrary to the I56T and D67H variants, the W64R variant has, however, not been purified from *ex-vivo* fibrils from patients bearing this mutation and therefore there is no definitive clue that the fibrils are made of the full-length protein. Moreover, no W64R protein was detected in the urine and plasma of the patients, under conditions where the wild-type protein was readily purified and characterized [6]. These results suggested that the W64R protein is present at a very low concentration in these bodily fluids. This finding could result from a high propensity of the full length W64R protein to form amyloid deposits [13]. Alternatively, it was hypothesised that the introduction of a charged residue into its hydrophobic core destabilized the protein and this may lead *in vivo* to its significant proteolysis into aggregation prone fragments [6]. In agreement with its possible low *in vivo* stability, the W64R protein could not be expressed as a heterologous protein in *Aspergillus niger*, while the I56T, D67H and WT lysozyme could [6]. These observations suggest that *in vivo* processing and turn-over of the W64R protein significantly differs from those of the previously characterized I56T and D67H amyloid variants [6].

Human lysozyme is a 130 amino acid residues protein that contains four disulphide bridges. It is made of two structural domains: the α-domain made of four helices and the β-domain which contains a β-sheet and a long loop (Fig. 1). The effects of two amyloidogenic mutations (I56T and D67H) and of the non-amyloidogenic mutation (T70N) on the *in vitro* properties of the protein have been investigated in detail, indicating that the amyloid formation originates from a significant reduction in the stability and global cooperativity of the protein structure. Consequently, both amyloidogenic variants are able to transiently populate partially unfolded species *in vitro* under physiologically relevant conditions. In these species, the β-domain and the C-helix are cooperatively and significantly unfolded, while the remaining α-domain exhibits a native-like structure [14–16] (Fig. 1). Interestingly, both the T70N variant and WT protein can also transiently populate such intermediate species but only if they are incubated in more destabilizing conditions (47 °C and 57 °C, respectively) [14,17]. These findings suggest that the ability of the β-domain and the C-helix to transiently partially unfold is an intrinsic property of the human lysozyme structure; whether or not a given mutational variant is associated with ALys critically depends, however, on the readiness with which this partial unfolding occurs *in vivo*.

In the present study, we report the production of the W64R protein into *P. pastoris* and we characterize the *in vitro* properties in terms of structure, stability and aggregation propensity in comparison to those of WT-HuL and of the I56T amyloidogenic variant. The results obtained indicate that the *in vitro* properties of the W64R protein are remarkably similar to those of the previously characterized I56T and D67H amyloidogenic variants. They further corroborate the idea that HuL variants associated with the disease are those whose stability and global structural cooperativity are sufficiently reduced to allow the formation of partially folded aggregation prone intermediates under physiological conditions.

2. Material and methods

2.1. Production and purification of proteins

A pPIC9 plasmid containing the gene of the I56T or W64R variant was used to transformed *P. pastoris* GS115 (Invitrogen) [18]. Both proteins were produced in a 15 L fermenter according to the protocol '*Pichia* Fermentation Process Guidelines' described from Invitrogen (https://tools.thermofisher.com/content/sfs/manuals/pichiaferm_prot.pdf) at the Protein Factory platform of the Centre of Protein Engineering (http://www.proteinfactory.ulg.ac.be). The protein is secreted into the culture medium which was recovered by centrifugation (7250 *g* for 15 min) and stored at −20 °C until the protein was purified. The supernatant was thawed, diluted 10 fold into 20 mM sodium acetate buffer pH 5.0, mixed with 70 mL of Sephadex SPFF resin (GE Healthcare, Uppsala, Sweden) and the mixture was stirred overnight at 4 °C. The resin was then recovered by filtration, poured into a column and the protein was eluted using a 700 mL linear gradient of NaCl (from 0 to 1.1 M) in 20 mM sodium acetate buffer pH 5.0, using an AKTA-prime system. The fractions containing proteins were analysed by SDS-PAGE (18%) and those containing lysozyme were pooled together and dialysed overnight against 50 mM Tris buffer pH 8.0. The protein was purified using an 8 mL Poros-HS column (Thermofisher Scientific, Waltham, MA, USA); the elution was carried out with a 50 mL linear gradient of NaCl between 0 and 1.1 M using an AKTA Explorer. The fractions containing protein were analysed by SDS-PAGE (18%) and those containing pure lysozyme were pool together, extensively dialysed against 0.1 M sodium acetate buffer pH 5.0. A part of the W64R protein co-eluted with a red pigment; thus, it was further purified using an IonTrap SP-HQ 5 mL column (GE Healthcare Europe GmbH, Sweden). The protein was eluted with a 20 mL linear gradient of NaCl from 0 to 1 M in 0.1 M sodium acetate buffer pH 5.0. Both lysozyme variants were finally desalted using a HiTrap Desalting 53 mL column (GE Healthcare Europe GmbH) with 0.1 M sodium acetate buffer pH 5.0. The proteins were filtered through a 0.22 μM membrane and stored at −20 °C at a concentration between 0.3 and 0.4 $g.L^{-1}$. Two independent batches of the W64R protein and one of the I56T protein were produced and purified. WT-HuL was bought from Sigma-Aldrich and further purified using on the Poros-HS column using the same protocol as described above. Upon thawing, if necessary the

proteins were concentrated by ultrafiltration.

2.2. Guanidinium chloride-induced unfolding

Samples of I56T, W64R and WT HuLs were incubated overnight at 25 °C in the presence of increasing concentrations of ultrapure guanidinium chloride (GdmCl, Sigma-Aldrich) in 0.1 M sodium acetate buffer pH 6.5. The protein concentration was 0.17 g·L^{-1} for the I56T and W64R variants and 0.2 g·L^{-1} for the WT protein. The denaturant concentration of each sample was determined from refractive index measurements [19], using a R5000 hand refractometer from Atago (Japan). Samples were used to measured intrinsic fluorescence and the far UV-CD signal at 222 nm as described below and then, 130 μL of a selected number of samples were mixed with 12 μL of ANS 11.3 mM. The [ANS]/[HuL] concentration ratio was about 80.

To check the reversibility of the unfolding process, two protein samples concentrated 10 times were prepared, one in the buffer (Native protein) and one in 6 M GdmCl (Denatured protein); and incubated 6 h at 25 °C. These two protein samples were then diluted into a series of tubes containing various concentrations of GdmCl (*e.g.*, 0.5, 1, 2, 3, 4 and 5 M) and incubated overnight at 25 °C to allow monitoring of the unfolding and refolding processes, respectively. The intrinsic fluorescence and far UV-CD spectra of each series were recorded and compared.

2.3. Fluorescence measurements

All fluorescence measurements were carried out using a Cary Eclipse Fluorimeter equipped with a thermostatically controlled multi-cuvette holder in a 10*1 mm pathlength quartz micro cuvette except where otherwise stated. The intrinsic fluorescence spectra to monitor changes in the tertiary structure were recorded at 25 °C from 300 nm to 440 nm after excitation at 295 nm with 5 nm excitation and emission slits. The voltage applied at the detector was 700 V. Data acquisition was made every 1 nm with a scan rate of 600 nm·min^{-1}. The spectra were not corrected by the absorbance value at 295 nm. The fluorescence spectra were fitted using a five parameter weibull function (from software SigmaPlot 5.0) to determine the wavelength corresponding to the highest fluorescence intensity (λ_{max}). ANS-bound fluorescence measurements were carried out recording the emission spectra from 420 nm to 600 nm after excitation at 350 nm with 5 nm excitation and emission slits. The voltage applied at the detector was 800 V. Data acquisition was made every 1 nm with a scan rate of 600 nm·min^{-1}. The fluorescence spectra were corrected for the background fluorescence of ANS alone.

2.4. Far UV-CD measurements

All the far UV-CD measurements were recorded using a Jasco J-810 spectropolarimeter equipped with a thermostatically controlled multi-cuvette holder. For the secondary structure analysis, far UV-CD spectra were recorded at 25 °C from 190 nm to 250 nm in a 0.2 mm pathlength cuvette. The protein concentration was 0.35 g·L^{-1} in 0.1 M sodium acetate buffer pH 6.5. The scan speed was set at 50 nm·min^{-1} and the D.I.T. was 2 s. Four scans were averaged, and corrected by subtraction of the buffer spectrum obtained under identical conditions. For the GdmCl-induced denaturation, the unfolding curves were monitored at 222 nm using a 1 mm pathlength quartz cuvette. At each denaturant concentration, 30 data points were acquired with a 2-nm bandwidth, a reading frequency of 1/15 s^{-1} and a 2 s integration time, and averaged. The resulting values were corrected for the contribution of the solution (buffer + GdmCl).

2.5. Heat-induced unfolding

Heat-induced unfolding transitions were monitored by far UV-CD at 222 nm in a 1 mm pathlength quartz cuvette and ANS-bound fluorescence at 480 nm in a 10*4 mm pathlength quartz cuvette, using a protein concentration of 0.2 g·L^{-1} in 0.1 M sodium acetate buffer pH 5.0. The temperature was increased monotonically at a rate of 0.50 °C·min^{-1} from 25 °C to 97 °C with data acquisition at each 0.25 °C. Mineral oil was added at the top of the samples to prevent their evaporation. The temperature was monitored with a thermocouple inserted in a cuvette containing only buffer. For far UV-CD measurements, data were acquired with a 4-s integration time and a 2-nm bandwidth. ANS-bound measurements were carried out at 480 nm following excitation at 350 nm; with 5 nm excitation and emission slits. The voltage applied at the detector was 800 V. The temperature corresponding to the maximum intensity peak of fluorescence emission was obtained by fitting the data with a Modified Gaussian, 5 Parameter model from SigmaPlot.

2.6. Data analysis of the GdmCl- and heat-unfolding transitions monitored by intrinsic fluorescence and far UV-CD

The changes in fluorescence intensity at 360 nm and in the CD signal at 222 nm were used to monitor the GmdCl-induced unfolding process. The transition curves obtained were analysed on the basis of a two-state (N ⇌ U) model according to Dumoulin et al. [20] and Eq. (1).

$$y_{obs} = \{(Y_N + p * [x]) + (Y_U + q * [x]) * \exp(-a)\}/(1 + \exp(-a)) \quad (1)$$

Where x is the concentration of denaturant and $a = (\Delta G_{NU}^{\circ}(H_2O) - m \times [D])/RT$, and where y_{obs} is the monitored fluorescence or CD signal at a given denaturant concentration, and Y_N and Y_U are the values of these signals for the native and denatured states in the absence of denaturant, respectively. $\Delta G_{NU}^{\circ}(H_2O)$ is the difference in free energy between the folded and unfolded conformations at 25 °C in the absence of denaturant; m is a measure of the dependence of the free energy on the denaturant concentration, and [D] is the denaturant concentration. p and q are the slopes of the pre- and post-unfolding baselines, respectively, R is the gas constant, and T is the absolute temperature. C_m, the denaturant concentration at the midpoint of the denaturation curve ([U]/[N] = 1) is defined as $\Delta G_{NU}^{\circ}(H_2O)/m$.

The heat-induced unfolding transitions monitored by the CD signal at 222 nm were used to determine the temperature of mid-transition (T_m) by fitting the experimental data with the eq. (1):

where x is the temperature and $a = (\Delta H_m(1 - x/T_m)Rx)$ [21] and y_{obs} is the CD signal at 222 nm at a given temperature, and Y_N and Y_U represent the CD signal for the native and denatured states at 273 K, respectively. T_m is the temperature of mid-transition and ΔH_m is the enthalpy value at T_m. Since the transitions were not fully reversible, only the (apparent) T_m value was considered. The fitting was carried out using Sigma plot.

2.7. Crystallisation and data collection

The W64R human lysozyme variant was concentrated to 14.4 g·L^{-1} in 10 mM Tris-HCl pH 7.0 and crystallized using the sitting-drop vapor diffusion method. 1 μL of protein was mixed with 1 μL of precipitant buffer (1.25 M $(NH_4)_2SO_4$, 0.1 M cacodylate pH 6.5) and crystals grew at room temperature. The crystals were transferred into a cryoprotectant solution containing 50% glycerol before flash-freezing in a liquid nitrogen bath. Diffraction data were collected at the Soleil Synchrotron Proxima 2a beamline (Paris). Data were integrated and scaled with XDS [22]. Initial phases were obtained by molecular replacement using the structure of WT human lysozyme as a search model (PDB code 1JSF [23]) using Phaser [24]. After substituting the tryptophan residue in position 64 with an arginine residue, further refinements were made using Phenix Refine [25]. The figures were prepared using PyMOL (The PyMOL Molecular Graphics System, Version 2.3.3 Enhanced for Mac OS X, Schrödinger, LLC.).

2.8. Limited proteolysis

WT, I56T and W64R lysozymes at 0.53 g·L^{-1} in a reaction volume of 200 µL were incubated in 50 mM Tris-HCl buffer pH 8.3 at 37 °C in the presence of proteinase K (Sigma Aldrich) at a protease-to-HuL molar ratio of 1:500. Aliquots of 20 µL were taken before the addition of the protease and then at different time intervals, and the proteolysis process was quenched by lowering the pH below 4 with the addition of 1.5 µL of 4% trifluoroacetic acid. The samples were mixed with 7 µL of 4 × sample buffer and then stored at −20 °C until analysis by SDS-PAGE using precast SDS-PAGE Stain-free 4–20% gels (Biorad). The gel was first imaged *via* the trihalo-bound tryptophan fluorescence (stain-free imaging), then it was stained by Coomassie blue and imaged again. The relative amount of intact protein was quantified by densitometry analysis with a Gel Doc EZ Imager (Biorad) using the intensity of the band at time zero as the relative standard. For a given time-point, the amounts of intact protein obtained from both imaging approaches were averaged.

2.9. Protein aggregation

The aggregation kinetics were monitored at 60 °C by right angle light scattering. The protein at 0.072 g·L^{-1} in 0.1 M sodium acetate pH 5.0 were incubated in a Cary Ellipse fluorimeter in 1 cm pathlength quartz cuvettes with stirring using a 6 mm × 2 mm magnetic bar. The light scattering was measured, each minute for three hours, at 500 nm, with excitation and emission slits of 5 nm, the voltage applied at the detector was 700 V. Occasionally, the solutions were manually inverted to avoid aggregates sedimentation in the cuvettes.

2.10. Transmission electron microscopy

Protein aggregates were analysed by transmission electron microscopy after staining with uranyl acetate. 10 µL of fibrils were loaded on a TEM grid previously exposed for 5 min to UV light at 312 nm. The excess of sample was removed and the grids let to dry; then the fibrils were stained with 10 µL of 2% uranyl acetate for 2 min. To remove excess of uranyl acetate, the grids were washed three times with 10 µL of H_2O and then dried. The aggregate solutions were analysed by transmission electron microscopy (TEM, Philips CM100) operating at 100 kV.

2.11. ThT-bound fluorescence emission spectra of fibrils

130 µL of ThT solution (50 µM) were mixed with 20 µL of fibrils in a 10*1 mm pathlength quartz micro-cuvette and the fluorescence spectrum was recorded using a Cary Ellipse fluorimeter, from 460 nm to 600 nm after excitation at 440 nm using both emission and excitation bandwidth of 5 nm. The voltage applied to the photomultiplier was 900 V. Eight spectra were averaged for each fibrils solution and corrected from the contribution of ThT alone.

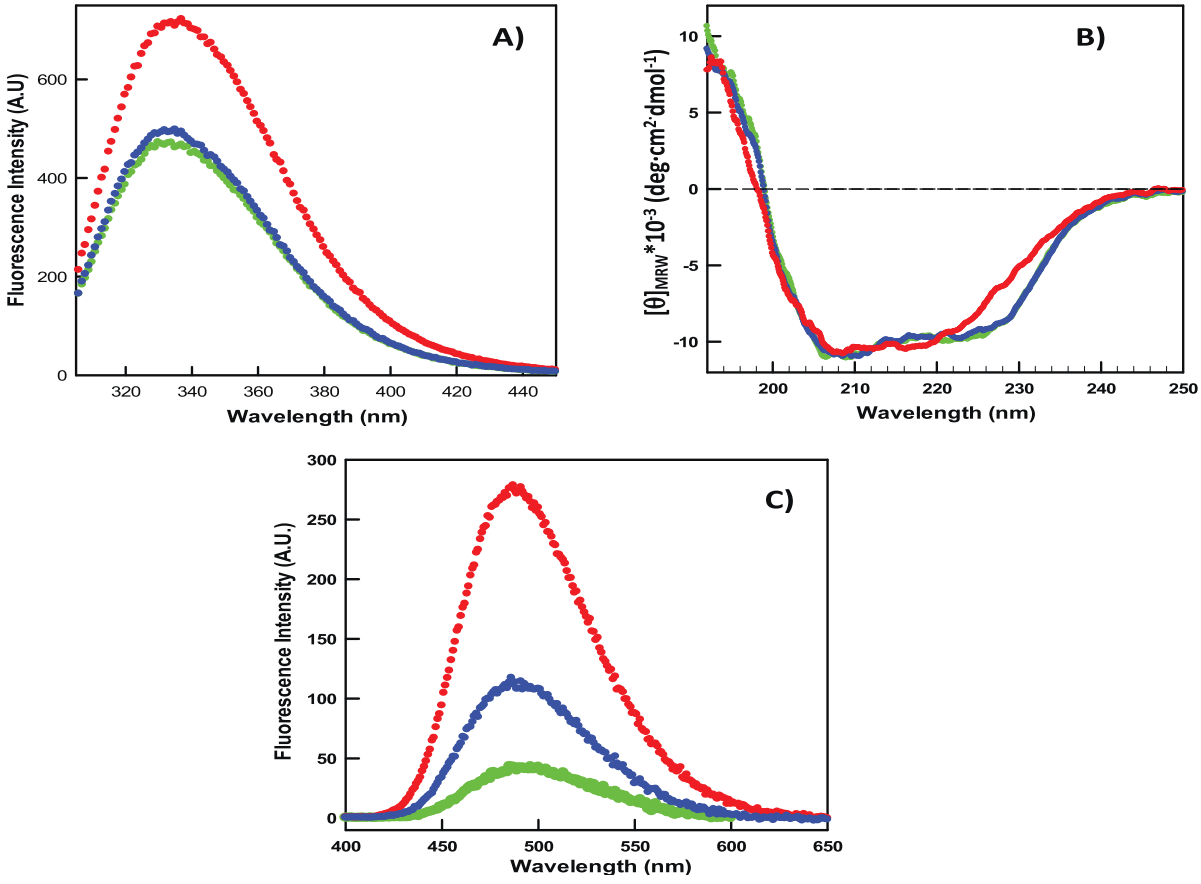

Fig. 2. Structural characterisation of the three lysozymes by fluorescence and far UV-CD. In (A-C): WT, green; I56T, blue and W64R, red. The protein concentration was 0.35 g·L^{-1} in 0.1 M sodium acetate buffer pH 6.5; all the spectra were recorded at 25 °C. A) Intrinsic fluorescence spectra. The spectra were recorded with a 10*1 mm pathlength quartz micro-cuvette, the excitation wavelength was 295 nm. The wavelength corresponding to the maximum in fluorescence intensity (λ_{max}) is 334.4, 334.1 and 336.3 nm, for the WT, I56T and W64R variants, respectively. B) Far-UV CD spectra. The spectra were recorded with a 0.2 mm pathlength quartz cuvette. The buffer spectrum was subtracted from all protein spectra. C) ANS-bound florescence spectra. The spectra were acquired with a 10*1 mm pathlength quartz micro-cuvette; the excitation wavelength was 350 nm. The voltage applied to the photomultiplicator was 800 V. The molar ratio [ANS]/[HuL] was 80. The spectrum of ANS alone was subtracted from all the sample spectra. (For interpretation of the references to colour in this figure legend, the reader is referred to the web version of this article.)

3. Results

3.1. Production of the W64R protein in P. pastoris

The W64R was expressed in *Pichia pastoris* in a 15 L fermenter at a yield similar to that obtained for the I56T, about 1.3 mg of pure protein was obtained per litre of culture. This result suggests that at least in the yeast *P. pastoris*, the *in vivo* processing of the W64R protein is not fundamentally different from that of the I56T protein.

3.2. Effects of the W64R mutation on the structure of the protein

3.2.1. Fluorescence and far UV-CD spectra

The effects of the W64R mutation on the tertiary structure of the protein were investigated by intrinsic fluorescence (Fig. 2A). The spectrum of the I56T protein is virtually identical to that of the WT-HuL. These results are in full agreement with the fact that the X-ray 3D structure of the two proteins are identical ($RMSD_{C\alpha} < 1$ Å) [26]. On the other hand, the spectrum of the W64R protein instead shows a significant red shift of the peak from 334 to 336 nm and an increased intensity. These changes have been observed for the spectra acquired with three different protein solutions prepared independently from different production batches and at protein concentrations ranging from 0.05 to 0.35 $g{\cdot}L^{-1}$. The increase in fluorescence intensity was unexpected since the W64R variant has one less tryptophan than the WT and I56T HuL. The shift of the wavelength corresponding to the maximum of fluorescence intensity (λ_{max}, which is independent of the protein concentration) suggests that at least one of the four remaining tryptophans within the W64R variant is more exposed to the solvent. The increase in intensity might be due to the reduction of a quenching effect resulting from the W64R substitution. According to the structure of the WT HuL and I56T HuL, W64 and W109 are parallel and separated by about 8 Å; a distance allowing tryptophan-tryptophan energy transfer [27] which would not occur anymore in the variant protein.

The effects of the mutation on the secondary structure of the protein were investigated by circular dichroism (CD) in the far-UV region (190–250 nm) (Fig. 2B). The spectrum of the I56T protein is indistinguishable from that of the wild-type protein, which again is in full agreement with the fact that the X-ray 3D structures of the two proteins are virtually identical. In comparison, the far UV-CD spectrum of the W64R protein clearly deviates from that of the WT protein and the I56T variant in the region between 222 and 240 nm. These differences are probably not associated with a loss of secondary structure as the minima at 208 nm and 222 nm remain at the same intensity for all the three lysozymes. The signal intensity decreasing around 230 nm happens in the region of the far-UV CD where aromatic residues highly contribute to the CD signal [28], thus the perturbation in the far UV-CD spectrum of the W64R protein is most likely due to the loss of W64 in favour of a non-aromatic residue, R64.

The ANS-bound spectra of the protein were also recorded (Fig. 2C). For all three proteins, a peak centred at 480 nm was observed indicating the presence of protein species at least partially unfolded exposing hydrophobic patches at their surface. The intensity of the peak is significantly higher for both amyloidogenic variants, and especially for the W64R protein. This suggests that the amount of partially unfolded species is significantly higher in the W64R sample. The presence of higher amount of this species could, at least in part, explain the changes in the intrinsic fluorescence spectrum of the W64R protein discussed above.

3.2.2. Crystal structure of the W64R HuL variant

The crystal used to collect the x-ray diffraction data belongs to the same space group ($P2_12_12_1$) and has approximately the same unit cell parameters as the WT HuL (PDB code 1JSF). The structure was solved, at 1.15 Å resolution by molecular replacement using the latter structure (Fig. 3). The coordinate file is deposited in the Protein Data Bank with the acquisition number 7AP7. The R_{cryst} and R_{free} values after refinement are 17.6% and 23.1% respectively (Table 1). The final electron density map shows a clear density for the whole protein except for the R122 and the C-terminus (residue 129 and 130).

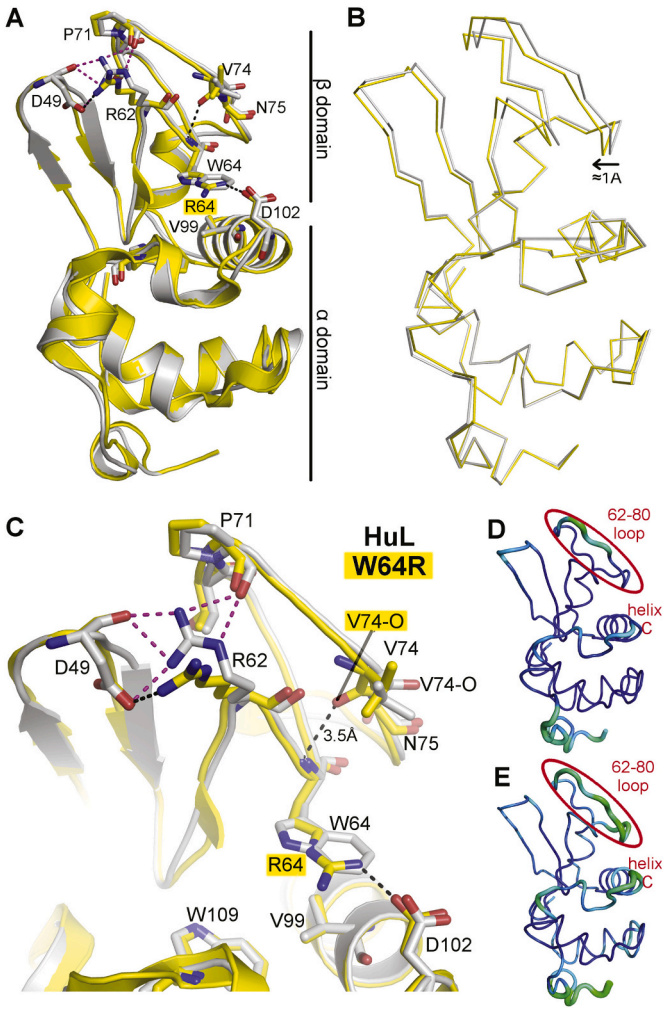

Fig. 3. Comparison of the structures of WT-HuL and its W64R variant. A) Cartoon representation of the WT-HuL (PDB code 1JSF, gray) and the superimposed W64R variant (yellow). Residues involved in differences between the structures are represented as sticks. Interactions of interest within WT-HuL and W64R variant are respectively shown as magenta and black dashed lines. B) Ribbon representations of the WT and W64R HuLs, with their α-domain superimposed, highlighting the slight β-domain shift. C) Same as A) with a close up view on the β-domain. D) Ribbon representation of the WT HuL structure (1JSF) with the rainbow colouring according to the B factor, blue low value and red high value. The ribbon thickness is also proportional to the B factor. E) Same as D for the W64R variant. (For interpretation of the references to colour in this figure legend, the reader is referred to the web version of this article.)

The W64R protein acquired the typical lysozyme fold with all the four disulphide bonds correctly formed (Fig. 3A) and with a global rmsd of 0.36 Å with the 1JSF WT HuL structure. The W64R mutation causes, however, a slight displacement of the β-domain (about 1 Å) when only the α domains are superimposed (Fig. 3B). The rmsd value is also slightly decreased to 0.3 Å over the 81 amino acids of this domain. The sidechain of the R64 substituting W64 adopts a remarkably similar orientation with all atoms of the arginine sidechain in the same plane as the W64 indole group (Fig. 3C). This orientation of the R64 sidechain also generates a salt bridge with the D102 sidechain, at least partially balancing the loss of hydrophobic interaction between W64 and V99 present in WT HuL at the interface between the β-domain and the C-helix. In addition,

Table 1
X-ray crystallographic data collection and refinement statistics. Values in parentheses refer to the high resolution shell.

	W64R human lysozyme
Data collection:	
Wavelength (C):	0.9801199
Space group:	$P2_12_12_1$
A, b, c (Å):	31.77, 56.66, 60.60
α, β, γ (°):	90, 90, 90
Resolution range (Å)	41.38–1.15 (1.17–1.15)
Rmerge	8.4 (76.9)
<I>/<σI>	10.04 (1.75)
Completeness (%)	98.7 (95)
Redundancy	6.35 (12.9)
CC1/2	0.99 (0.79)
Refinement:	
Resolution range (Å)	30.29–1.15
No of unique reflections	39,365
R work (%)	16
R free (%)	19.3
No. of non-hydrogen atoms	1261
Number of water molecules	164
RMS deviations from ideal stereochemistry	
Bond lengths (Å)	1.05
Bond angles (°)	1.13
Mean B factor (Å^2)	
Protein	12.3
Water	45.09
Ramachandran plot:	
Favoured region (%)	97
Allowed regions (%)	3
Outlier regions (%)	0

the W64R mutation slightly modifies one of the two side-chain hydrogen bonding networks that is thought to stabilize the β-domain of the WT protein [11]. Indeed, the peptide bond between V74 and N75 displays a 180° flip compared to its position in the WT-HuL and R62 no longer interacts with the backbone carbonyl of D49 and P71 (Fig. 3C). The peptide bond flip, which is adjacent to R64 (3.5 Å between the V74 carbonyl oxygen and amide nitrogen of R64), is well defined in the electron density map. The R62 sidechain has been observed in a similar orientation in the T70N variant, where it is directly adjacent to the T70N substitution. In the W64R structure, the R62 sidechain is interacting with a SO_4^{2-} molecule that results from the use of $(NH_4)_2SO_4$ for the crystallisation instead of the NH_4NO_3 used for most HuL crystallographic structures. Moreover, a comparison of the B factors of the W64R and WT HuL (PDB code 1JSF) structures, both solved at the same resolution (1.15 Å), shows a local increase of the B factor of the 62–80 loop and the C-terminal end of helix C around the D102 position for the W64R variant (Fig. 3D and E), suggesting that these regions are more flexible. All together, these subtle modifications are enough to sufficiently destabilize the protein and reduce the global cooperativity to allow the partial unfolding to occur, as demonstrated below by a series of techniques.

3.3. Effects of the W64R mutation on the stability of the protein

3.3.1. Heat-induced unfolding

The thermostability of the W64R protein was monitored by far UV-CD at 222 nm and ANS-bound fluorescence (Fig. 4) and compared to those of the I56T and WT proteins. By far UV-CD, a single sigmoidal transition is observed suggesting that the thermal unfolding of the secondary structures occurs *via* a two-state model, as was observed for the I56T and WT proteins (data not shown). The apparent temperature of the mid-point of unfolding (T_m) of the W64R protein is similar to that of I56T and D67H variants (64 °C *versus* 68 °C, Table 2). This value is about 13 °C lower than that of the wild-type protein, ($T_m \sim 77$ °C) under similar conditions. The heat-induced unfolding was also monitored by ANS-bound fluorescence (Fig. 4 B). At 25 °C, the three proteins bind ANS (W64R > I56T > WT) as it was observed in Fig. 2C; suggesting again that they populate partially folded intermediates, although in very small amounts. Then, the ANS-bound fluorescence decreases as the temperature increases up to about 40 °C suggesting that the partially unfolded species initially present in the solutions are denatured at these rather low temperatures. These unfolding events are not observed by far UV-CD (Fig. 4A for the W64R protein, and data not shown for the I56T and WT proteins), demonstrating again that the amounts of such species are very low. At higher temperature, the increase in ANS-bound fluorescence is associated with the denaturation of the native proteins into partially unfolded intermediates. The peak of fluorescence is centred around the respective T_m of each protein (Fig. 4B) (Table 2). The amount of intermediate species formed by the I56T and W64R proteins is significantly higher than that formed by the WT protein.

3.3.2. Guanidinium-induced unfolding

The stability of the W64R protein was investigated by GdmCl-induced unfolding (Fig. 5) and was compared to those of the WT and I56T proteins. The unfolding and refolding processes are superimposable throughout the transition, confirming the reversibility of the unfolding process for the three proteins (data not shown). A single transition was obtained for the W64R protein monitored by either intrinsic fluorescence (Fig. 5B) or far UV-CD (Fig. 5A) as well as the I56T and WT-HuL (data not shown). The transition curves obtained by intrinsic fluorescence and far UV-CD measurements (Fig. 5D) for the W64R and WT proteins almost perfectly overlap indicating that their secondary and tertiary structures are destabilized coincidently. For the I56T variant, the unfolding transition was monitored only by intrinsic fluorescence, the cooperative unfolding of the secondary and tertiary unfolding was however reported previously [29]. The unfolding of the three proteins occurs therefore *via* a cooperative two-state model (N ⇌ U), in which only the native and unfolded states are significantly populated. Based on this model, the Gibbs free energy of unfolding $\Delta G^0_{NU}(H_2O)$, the *m*-value and GdmCl concentration at mid-transition (C_m) were calculated and are given in Table 3. Within the error limit, the $\Delta G^0_{NU}(H_2O)$) values are identical for both optical methods. Moreover, for both the WT-HuL and the I56T proteins, the values are in good agreement to those described in literature [29–31]. The W64R variant is destabilized compared to the WT protein by about 24 kJ·mol^{-1}. Remarkably, the stability of the W64R protein is very similar to that of the I56T protein, while it is lower than that of the D67H protein (Table 3). In comparison, previous studies indicated that the non-amyloidogenic T70N variant is not destabilized as much as any of the three amyloidogenic lysozymes [17,31] (Table 3). The GdmCl unfolding transitions have also been monitored by ANS-bound fluorescence (Fig. 5C). Contrary to what was observed in Fig. 2, very low ANS-bound fluorescence is observed at 25 °C in the absence of denaturant for the three proteins; thus, it is likely that the partially folded species initially present in the samples have been denatured during the overnight incubation of the sample at 25 °C (see M&M) explaining why low ANS-bound fluorescence is observed for the amyloidogenic variants and the WT protein, respectively. An increase in the ANS-bound fluorescence intensity at GdmCl concentrations close to their respective C_m (denaturant concentration at mid-transition) was observed for both the I56T and W64R proteins. This indicates that these proteins populate a small amount of partially unfolded state although it was too small to be detected by fluorescence and CD. Indeed, the signals of intrinsic fluorescence and far UV-CD result from the weighted sum of the signal of each individual species present in the solution, *e.g.*, native, unfolded and intermediate species. The fact that the transition curves monitored by intrinsic fluorescence and far UV-CD are almost fully overlapping indicates that the amount of intermediate is very small and does not contribute significantly to the overall fluorescence or far UV-CD signal. Thus, the results suggest that for the W64R protein (as for the amyloidogenic variants I56T and D67H) the amount of intermediate formed is too low to be detected with these techniques. On the other hand, the

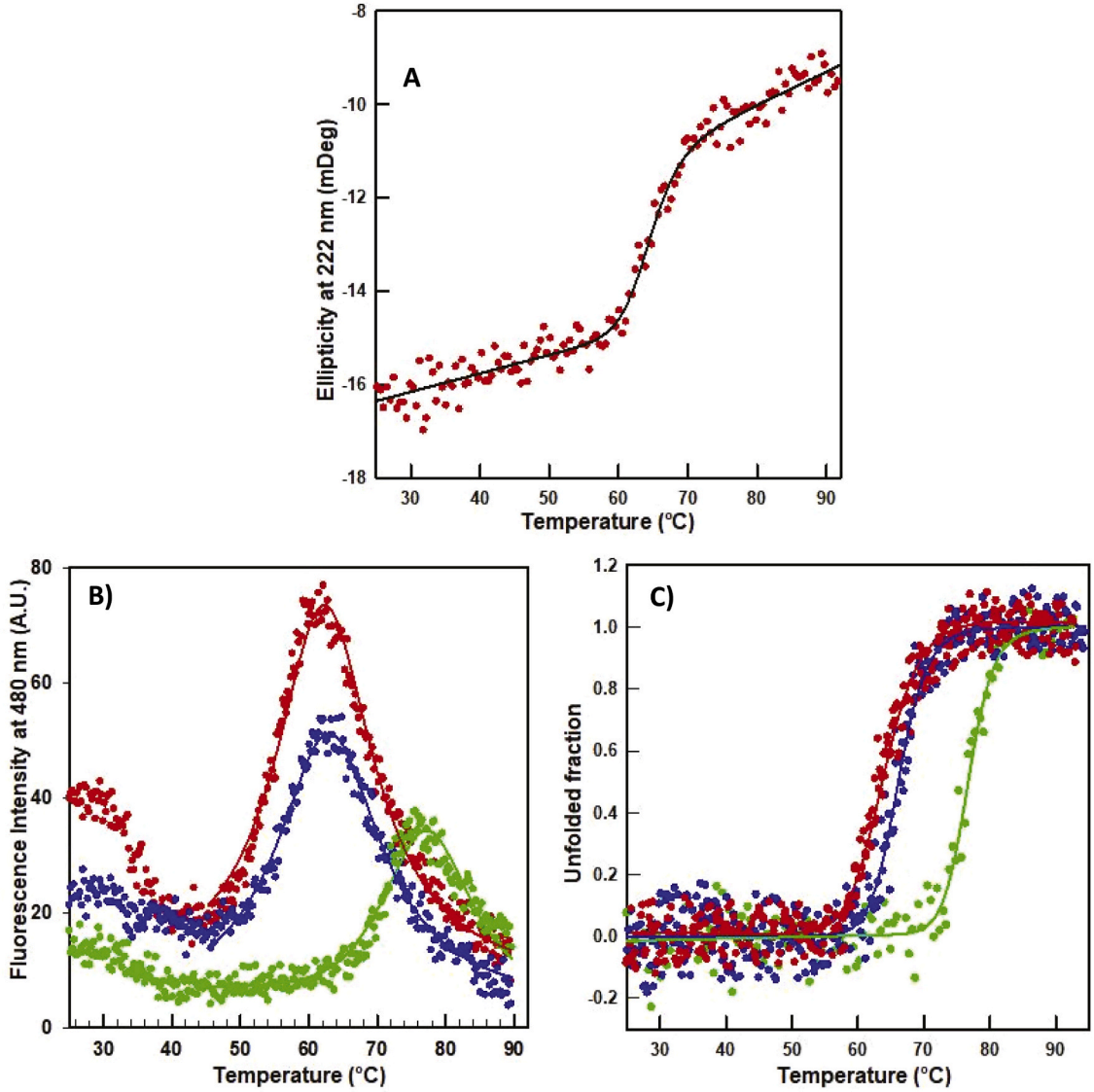

Fig. 4. Thermal unfolding of the three lysozymes monitored by far UV-CD at 222 nm in a 1 mm pathlength cuvette (A) and ANS-bound fluorescence at 480 nm in a 10*4 mm pathlength cuvette (B). Red, W64R; Blue, I56T; Green, WT. The protein concentration was 0.2 g·L^{-1} in 0.1 M sodium acetate buffer pH 5.0. Data in A were analysed on the basis of a two-state model, and the lines represents the best fit to Eq. (1). The solid line in B corresponds to the fit of the experimental data using a Modified Gaussian, 5 Parameter model from SigmaPlot. (C) Unfolded fraction of the three proteins, F_U, as a function of the temperature. The F_U values were calculated from data obtained by far UV-CD at 222 nm. The lines represent the best fit using Eq. (1). (For interpretation of the references to colour in this figure legend, the reader is referred to the web version of this article.)

Table 2
Thermal stability of the WT, I56T and W64R lysozymes at pH 5.0, derived from the analysis of the heat-induced equilibrium transitions monitored by far UV-CD and ANS-bound fluorescence.

Proteins	T_m (°C) ANS-bound fluorescence	T_m (°C) Far-UV CD
WT	76.5 ± 0.9	76.7 ± 0.4
W64R	61.8 ± 0.7	64.0 ± 1.0
I56T	63.2 ± 0.4	67.6 ± 1.0
D67H[a]	66.0 ± 2.0	68.0 ± 1.0
T70N[b]	74.0 ± 0.6	74.8 ± 1.0

Note that since the thermal unfolding was not fully reversible, the T_m actually corresponds to the apparent T_m. The values reported are the average of two independent measurements.

[a] From [16].

[b] From [18].

signal measured by ANS fluorescence is only due to the partially unfolded species, thus this technique is able to detect much lower amount of intermediate species.

3.4. Effects of the W64R mutation on the dynamics of the protein

As mentioned previously, the W64R protein was not detectable in urine or in plasma samples suggesting that it might be degraded [6]. On the other hand, the D67H protein could be detected in the urine and it was found to be included in amyloid fibrils as full-length protein [26]. In order to determine whether the W64R protein was indeed more prone to proteolysis, we compare the *in vitro* hydrolysis by proteinase K to that of the I56T and WT proteins. Proteinase K was chosen because it shows a broad substrate specificity and its ability to hydrolyse a given protein is therefore not associated with the presence of a specific amino acid sequence. Proteolysis depends instead on the protein substrate's overall structure and dynamics since it will occur only if the polypeptide chain is

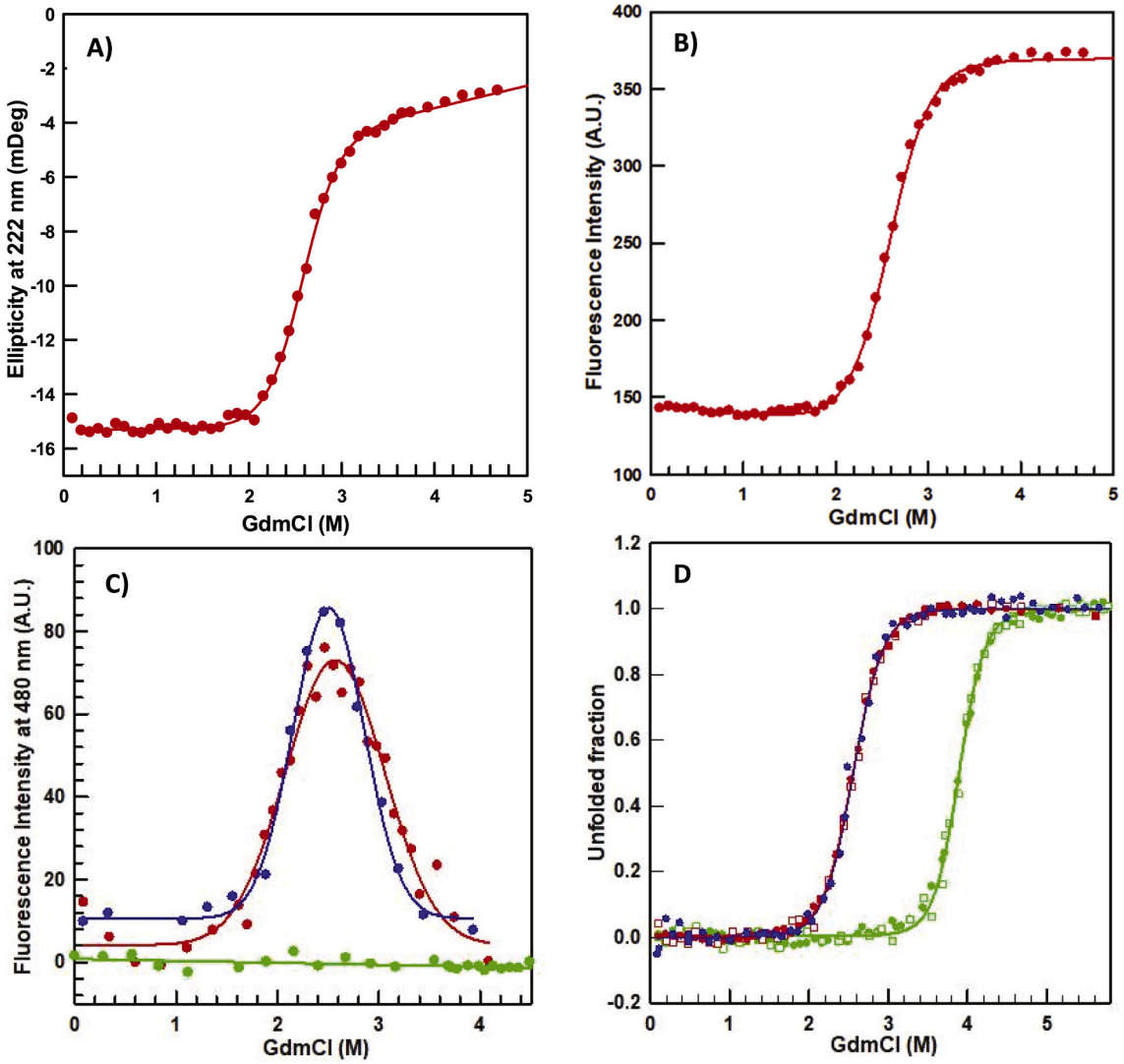

Fig. 5. GdmCl-induced unfolding transitions. Transitions monitored for the W64R variant by A) far UV-CD at 222 nm using a 1 mm pathlength quartz cuvette, B) intrinsic fluorescence at 360 nm using a 10*1 mm pathlength quartz micro-cuvettef and C) ANS-bound fluorescence at 480 nm using a 10*1 mm pathlength cuvette. In (A–D): WT, green; I56T, blue and W64R, red. The protein concentration was 0.17 g·L^{-1} for the I56T and W64R variants and 0.2 g·L^{-1} for the WT protein. In A & B, the solid lines represent the best fit calculated using the thermodynamic values in Table 3. The solid lines in C, correspond to the fit of the experimental data using a Modified Gaussian, 5 Parameter model from SigmaPlot. D) Normalised transition for the three proteins monitored by intrinsic fluorescence signal at 360 nm (full circles) and far UV-CD at 222 nm (empty squares). The solid lines represent the best fit calculated using the thermodynamic values in Table 3. (For interpretation of the references to colour in this figure legend, the reader is referred to the web version of this article.

able to be accommodated into the active site of the enzyme; and this later event requires that a stretch of 8 to 10 residues of the polypeptide chain is accessible to the active site of enzyme [32]. Thus, local unfolding of a polypeptide chain can be detected *via* the use of proteinase K. In the absence of the protease, none of the lysozyme variants were degraded within 24 h (data not shown). However, in the presence of protease (500:1 M ratio of lysozyme-to-protease), the W64R and I56T proteins were completely degraded within 24 h at a similar rate while the WT protein remains intact (Fig. 6); this latter result is in agreement with previous studies [32]. These observations suggest that the amyloidogenic variants populate transiently unfolded states, which allow the cleavage sites to be exposed to the protease. Two protein fragments are observed upon proteolysis whose sizes are in agreement with those observed with pigeon and dog lysozymes under similar conditions [32]. These fragments do not, however, accumulate over time suggesting that they are further digested after the initial cleavage occurs.

3.5. *Effects of the W64R mutation on the aggregation of the protein*

The propensity of the W64R HuL to form fibrils was compared to that of the I56T protein by monitoring the formation of aggregates by right angle light scattering under conditions that were previously used to trigger the aggregation into amyloid fibrils of the full-length lysozyme [16], *i.e.* at pH 5.0 and 60 °C. The kinetic of aggregation of each protein show the existence of a lag phase followed by rapid growth. This behaviour is typical of a nucleated process and it was observed previously for the I56T, D67H and a series of non-naturally occurring HuL variants [16,17,29,33]. The lag-phase lasts for 10–15 min and 20–25 min for W64R and I56T variants, respectively (Fig. 7). The aggregation progresses faster for the W64R than for the I56T variant under these conditions. This can be explained by the fact that at 60 °C, the amount of intermediate species is slightly higher for the W64R protein than for the I56T HuL (Fig. 4B). TEM analysis of the aggregates confirmed that the W64R variant forms fibrils of similar appearance than those formed by the I56T variant (Fig. 7 C&D). Moreover, the fibrils formed by the W64R

Table 3
Thermodynamic parameters derived from the analysis, based on a cooperative two-state model (N ⇌ U), of the GdmCl-induced unfolding equilibrium transition of the WT, I56T and W64R lysozymes at pH 6.5, 25 °C.

Proteins	$\Delta G^{\circ}_{NU(H2O)}$ (kJ·mol^{-1})	m(kJ·mol^{-1} M^{-1})	C_m (M)
WT			
Far UV-CD	59.4 ± 3.2	13.7 ± 0.7	4.3 ± 0.3
Int. Fluo	53.2 ± 1.9	12.3 ± 0.4	4.3 ± 0.2
Average	56.3 ± 4.3	13.0 ± 1.0	4.3 ± 0.1
I56T			
Int. Fluo	33.7 ± 2.1	13.2 ± 0.8	2.6 ± 0.2
W64R			
Far UV-CD	32.2 ± 1.3	12.6 ± 0.5	2.6 ± 0.1
Int. Fluo	32.7 ± 0.9	12.8 ± 0.4	2.6 ± 0.1
Average	32.4 ± 0.3	12.7 ± 0.2	2.6 ± 0.05
D67H[a]			
Int. Fluo	37.6	ND	2.8
T70N[a]			
Int. Fluo	41.8	ND	3.4

ND, not reported.
[a] From Esposito et al. [31].

variant bind THT similarly to those formed by the I56T variant (Fig. 7B).

4. Discussion

Amyloidoses are characterized by the deposition of highly organized fibrillar aggregates made of specific proteins or peptides in various tissues including the brain, kidney and heart [34]. They constitute an enormous health challenge for the developed world where their prevalence increases rapidly due to the ageing population and their lifestyle. Understanding how proteins or peptides acquire the amyloid conformation is of crucial importance to establishing therapeutic strategies. Human lysozyme amyloidosis is a hereditary non-neuropathic systemic amyloidosis associated with the misfolding and aggregation of mutational variants of the protein into amyloid fibrils that deposit in various vital organs including the liver, spleen, and kidney [1,3,13]. Up to now, six single and two double mutational amyloidogenic variants of the protein have been reported [1,3,13]. Although the number of affected people worldwide is limited compared to other amyloidoses (*i.e.*, about 30 families [8]), human lysozyme is of particular interest in understanding the mechanism by which a globular protein converts into amyloid fibrils. Indeed, not only has the WT protein been used as a model to extensively study protein folding and stability as previously reviewed [1,2,13], but amyloidogenic and non-amyloidogenic natural variants have also been identified. Thus, a detailed comparison of the properties of two amyloidogenic (I56T and D67H) and one non-amyloidogenic (T70N) proteins to those of the WT protein has allowed the mechanism of aggregation to be proposed at the molecular level. The results of these studies indicate the stability of the native state of both amyloidogenic variants and their global structural cooperativity is reduced to a very similar extent relative to the WT protein. It was therefore proposed that these reductions are the determining features underlying their amyloidogenicity. Indeed, hydrogen/deuterium exchange experiments analysed by mass spectrometry and NMR show that both amyloidogenic variants can populate transiently, under physiologically relevant conditions (pH 6.1–8.2 and 37 °C [14]), partially folded species in which their β-domain and the adjacent C-helix are unfolded, whereas the rest of the α-domain maintains its native state [14,16]. The association process that eventually results in the formation of amyloid fibrils is likely to be initiated by the formation of intermolecular interactions between the unfolded regions of the protein in such intermediate species [14,15,35]. Camelid antibody fragments (referred to as V_HHs or Nanobodies) are unique probes to dissect the mechanism of fibril formation [36]. For example, we have shown that the binding of two Nanobodies specific for HuL (*i.e.* cAb-HuL6 and cAb-HuL22), is a very effective strategy to restore global structural cooperativity of the amyloidogenic variants and thus to inhibit their conversion into amyloid fibrils [15,16,37]. These observations support the causative link between the reduction in the structural cooperativity between the α- and β-domains and the ability to form amyloid fibrils under physiological conditions.

In this study, we compared the properties of the W64R variant of human lysozyme in terms of structure, stability, dynamics and aggregation propensity to those of the I56T and WT proteins. Based on the fact that (i) no W64R protein could be detected in the urine and the serum of patients and (ii) it could not be produced in *A. niger* while the I56T and D67H could, it was suggested that the replacement of the W64 by an arginine was highly destabilizing and thus highly prone to degradation into aggregation prone peptides *in vivo* [6]. In the present study, the protein could be expressed in *P. pastoris* in amounts similar to the I56T

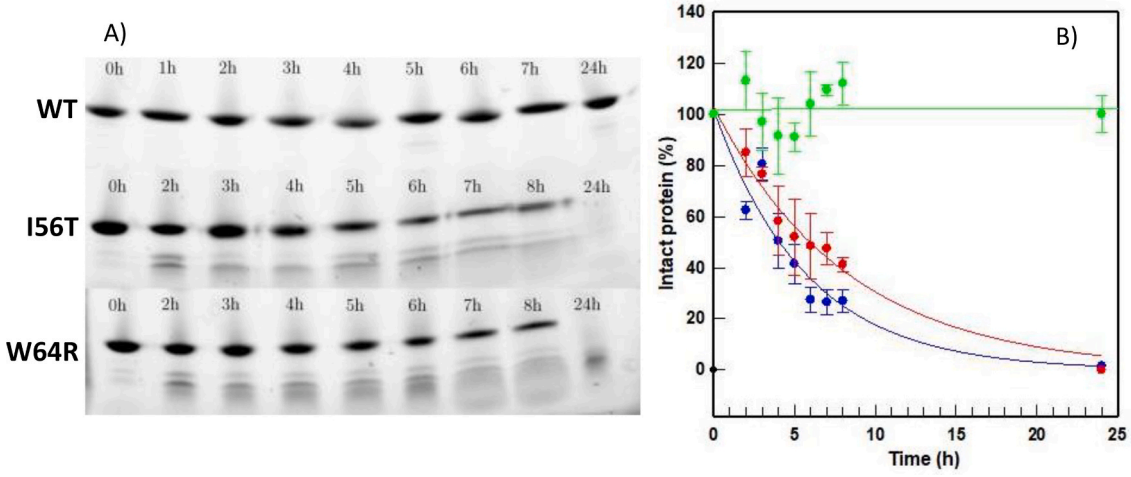

Fig. 6. Limited proteolysis analysed by SDS-PAGE. A) SDS-PAGE analysis of the limited proteolysis reaction products of WT, I56T and W64R HuL on a 4–20% precast stain-free gel. Aliquots were taken from the reacting solution at various times intervals and 4% TFA was added to stop the reaction. After 24 h only the full length WT-HuL is present, while there are no more traces of the intact I56T and W64R variants. B) Degradation kinetics of HuLs by proteinase K. The relative intensity of the bands was derived from densitometry analysis of the gels using a Biorad GelDoc EZ system. WT-HuL (green), W64R variant (red) and I56T (blue). The values reported are the average of those obtained from the analysis of the gels imaged *via* trihalo-bound tryptophan fluorescence and *via* Coomassie blue. (For interpretation of the references to colour in this figure legend, the reader is referred to the web version of this article.)

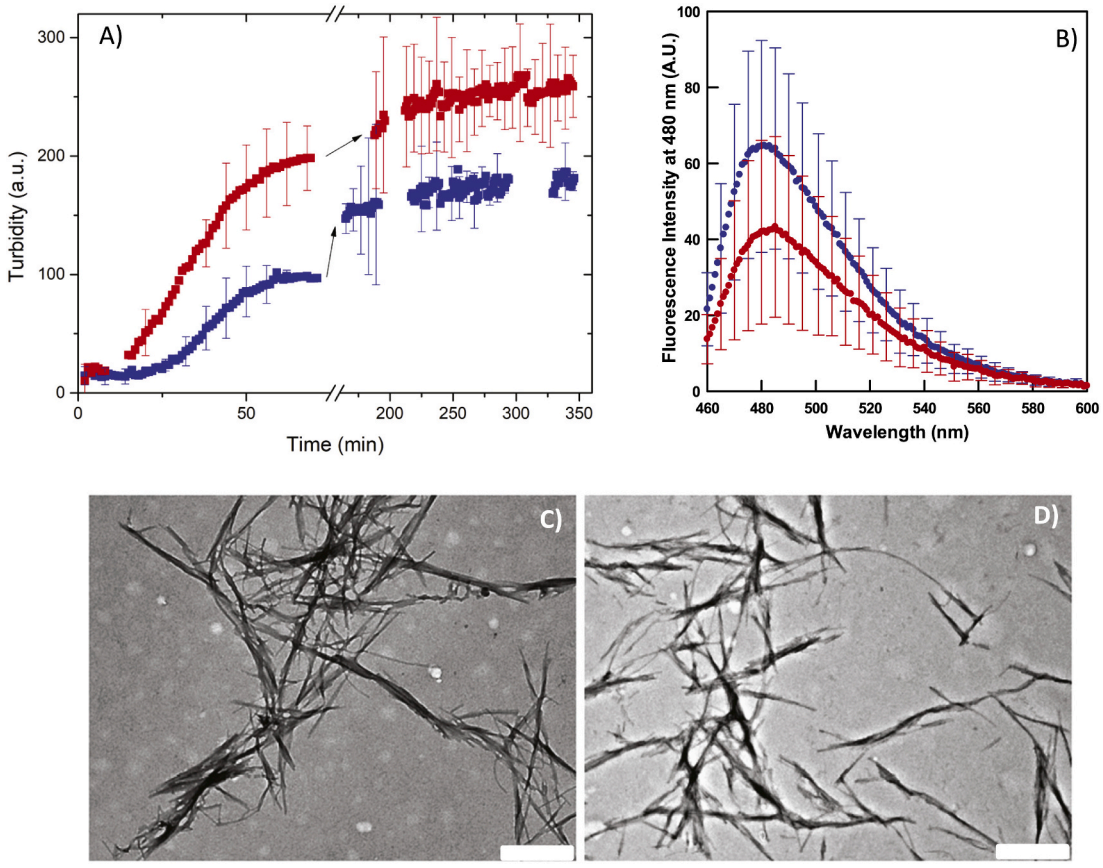

Fig. 7. Time course of aggregation of the W64R (red) and I56T (blue) variants of human lysozyme. A) The aggregation was monitored by light scattering at 500 nm at 60 °C with a protein concentration of 0.072 g·L^{-1} in 0.1 M sodium buffer pH 5.0. The experiment was carried out in duplicate and the average is shown, with the error bars indicating the standard deviation. B) ThT-bound fluorescence of the aggregates formed. Fibril solutions were mixed with a solution of 50 μM ThT. The experiment was carried out in duplicate and the average is shown, with the error bars indicating the standard deviation. C&D) Representative images of fibrils formed by the W64R (C) and I56T (D) lysozymes and observed by TEM. The scale bars represent 500 nm. (For interpretation of the references to colour in this figure legend, the reader is referred to the web version of this article.)

protein, indicating that at least in this organism the *in vivo* behaviour of the two variants are similar. The X-ray structure of the W64R variant is very similar to that of the WT protein and the I56T variant. The main differences are (i) a slight displacement (about 1 Å) of the β-domain when the α-domains are superimposed, (ii) the replacement of the hydrophobic interaction between W64 and V99 by a salt bridge between R64 and D102 at the interface between the α- and β- domains, and (iii) the disruption a few hydrogen bonds of one of the two side-chain hydrogen networks that stabilize the β-domain in the WT protein. The amyloidogenic D67H and the non-amyloidogenic T70N mutations, that are located on the same loop as W64R, also induce a significant movement (RMSD$_{C\alpha}$ up to 11 Å) of the β-sheet structure and particularly the region containing residues 42–55 and 66–75, although in this case the two loops move apart from each other [17,26]. Being observed for amyloidogenic and non-amyloidogenic variants, such structural movements do not, therefore, constitute by themselves a critical factor underlying the amyloidogenic character of a given mutation. In the D67H protein, both hydrogen networks stabilizing the β-domain are almost completely disrupted by the backbone rearrangement with effects transmitted to the interface between the α- and β-domains [26]. As a result, I56 adopts the conformation of a different rotamer and the indole ring of W64 moves away from the C-helix. In the I56T protein, none of the hydrogen bond network is affected and the greatest effect of the mutation is the disruption, at the domain interface, of interactions formed in the WT protein by the I56 side-chain [26]. In the native state of the T70N protein, most of the WT hydrogen bonds are formed although a few individual hydrogen bonds are disrupted. Moreover; the interface is only slightly modified by the T70N mutation: the I59T adopts a different rotamer but the sidechains of I56 and W64 are in the same conformation as in the WT protein [17]. In the W64R protein, the few individual hydrogen bonds that are disrupted are very similar to those that are disrupted in the T70N protein. The side chain of I56 and F57 at the interface are in their native conformation; thus the greater destabilisation of the W64R is likely due to the fact that the new salt bridge between R64 and D102 does not fully compensate for the loss of the hydrophobic interaction at the interface between the α- and β-domain. The far-UV-CD and intrinsic fluorescence measurements in native conditions indicate that also in solution, the W64R adopts a fold very similar to that of the WT and I56T proteins. The ANS-bound fluorescence experiments indicate, however, that under such conditions, the W64R protein populates an intermediate species in larger amounts than the I56T and the WT protein. This effect can however not be seen by crystallography because the crystallisation process likely acts as a selection process for the properly folded protein. Equilibrium denaturation unfolding experiments show that the extent of the destabilisation is almost identical for the W64R and I56T variants, with a $\Delta\Delta G^{\circ}_{NU}(H_2O)$ compared to WT-HuL of 24 kJ·mol^{-1}; a similar destabilisation was also observed for the D67H variant while the T70N protein is significantly less destabilized. The thermal stability of the three amyloidogenic variants is also decreased to a similar extent and more than that of the T70N protein. The W64R and I56T proteins populate an intermediate species in significantly higher amounts close to their respective C_m and T_m. Moreover, both the W64R and D67H proteins are amendable to proteinase K hydrolysis upon incubation at 37 °C, while the WT protein is

not. It was previously demonstrated that the sites of initial proteolytic cleavages of lysozymes from different species occur at the level of the β-domain (in the region 34–57) [32]. These observations are in very good agreement with hydrogen/deuterium (H/D) experiments in native conditions monitored by mass spectrometry and NMR, which have shown that the I56T and D67H proteins populate transiently partially folded intermediate in which the β-domain and the C-helix are unfolded while the rest of the α-domain maintains its native structure [15,16]. Such transient partial unfolding is most likely the event that allows the proteolysis of the I56T amyloidogenic variant by proteinase K. The similar proteolytic cleavage profile of the W64R variant to that of the I56T protein suggests, therefore, that the W64R protein transiently populates a similar intermediate as the I56T and D67H variant in physiologically relevant conditions. H/D experiments monitored by NMR and mass spectrometry should, however, be carried out to confirm that. Finally, the *in vitro* propensity of the W64R protein to aggregate into amyloid fibrils is very similar to that of the I56T protein. Overall, these results show that the *in vitro* properties of the W64R variant are remarkably similar to those of the I56T and D67H proteins.

Previous studies involving a series of non-natural variant bearing a mutation at different locations of the protein have demonstrated that the ability to form a partially unfolded intermediate, in which the β-domain and C-helix are essentially unfolded, is a generic properties of the lysozyme fold [29,33]. However, only the naturally occurring amyloidogenic single-point mutations trigger the formation of such intermediate species in significant amounts under physiologically relevant conditions. Interestingly, the amyloidogenic mutations are all located in the β-domain of lysozyme suggesting that the location of the mutation is crucial in determining the amyloidogenic character of the protein. In support of this, it was observed that among non-natural variants having similar native state stability, those carrying a mutation in the α-domain have a significantly lower ability to transiently populate intermediate species under physiologically relevant conditions. Moreover, a variant bearing a mutation at the interface (*i.e.*, I56V) more efficiently populates a transient intermediate species at elevated temperatures than variants bearing more destabilizing α-domain mutations [33].

5. Conclusion

Altogether, the results obtained in this study indicate that the *in vitro* properties of the W64R protein are remarkably similar to those of the previously characterized I56T and D67H amyloidogenic variants. They further corroborate the idea that HuL variants associated with the disease are those whose stability and global structural cooperativity are sufficiently reduced to allow the formation of aggregation prone partially folded intermediates under physiological conditions as a result of a greater disruption of stabilizing interactions in the β-domain and/or at the interface region.

Declaration of Competing Interest

None.

Acknowledgements

This work was carried out in the frame of an ERASMUS exchange between the University of Padova (Italy) and the University of Liège. M. D. and F·K are Research Associates of the National Fund for Scientific Research (F.N.R.S., Belgium). The authors are grateful for the assistance and support of the proxima 2a beamline scientists at the Soleil synchrotron. We acknowledge the assistance of F. Bouillenne for the purification of the proteins.

References

[1] M. Dumoulin, J.R. Kumita, C.M. Dobson, Normal and aberrant biological self-assembly: insights from studies of human lysozyme and its amyloidogenic variants, Acc. Chem. Res. (2006), https://doi.org/10.1021/ar050070g.
[2] M. Dumoulin, Familial amyloidosis caused by lysozyme, in: Protein Misfolding Dis. Curr. Emerg. Princ. Ther, 2010, https://doi.org/10.1002/9780470572702.ch39.
[3] M. Dumoulin, V. Bellotti, C.M. Dobson, Lysozyme, in: Amyloid Proteins Beta Sheet Conform. Dis, 2008, https://doi.org/10.1002/9783527619344.ch24.
[4] S.H. Nasr, S. Dasari, J.R. Mills, J.D. Theis, M.T. Zimmermann, R. Fonseca, J. A. Vrana, S.J. Lester, B.M. McLaughlin, R. Gillespie, W.E. Highsmith, J.J. Lee, A. Dispenzieri, P.J. Kurtin, Hereditary lysozyme amyloidosis variant p.Leu102Ser associates with unique phenotype, J. Am. Soc. Nephrol. (2017), https://doi.org/10.1681/ASN.2016090951.
[5] M.B. Pepys, P.N. Hawkins, D.R. Booth, D.M. Vigushin, G.A. Tennent, A.K. Soutar, N. Totty, O. Nguyen, C.C.F. Blake, C.J. Terry, T.G. Feest, A.M. Zalin, J.J. Hsuan, Human lysozyme gene mutations cause hereditary systemic amyloidosis, Nature (1993), https://doi.org/10.1038/362553a0.
[6] S. Valleix, S. Drunat, J.B. Philit, D. Adoue, J.C. Piette, D. Droz, B. Mac Gregor, D. Canet, M. Delpech, G. Grateau, Hereditary renal amyloidosis caused by a new variant lysozyme W64R in a French family, Kidney Int. (2002), https://doi.org/10.1046/j.1523-1755.2002.00205.x.
[7] S. Girnius, M. Skinner, B. Spencer, T. Prokaeva, C. Bartholomew, C. O'Hara, D. C. Seldin, L.H. Connors, A new lysozyme tyr54asn mutation causing amyloidosis in a family of Swedish ancestry with gastrointestinal symptoms, Amyloid (2012), https://doi.org/10.3109/13506129.2012.723074.
[8] Z. Li, H. Xu, D. Liu, D. Li, G. Liu, S.X. Wang, Hereditary renal amyloidosis with a variant lysozyme p.Trp82Arg in a Chinese family: case report and literature review, BMC Nephrol. 20 (2019), https://doi.org/10.1186/s12882-019-1496-6.
[9] D.R. Booth, M.B. Pepys, P.N. Hawkins, A novel variant of human lysozyme (T70N) is common in the normal population, Hum. Mutat. (2000), https://doi.org/10.1002/1098-1004(200008)16:2<180::aid-humu20>3.0.co;2-%23.
[10] C. Röcken, K. Becker, M. Fändrich, V. Schroeckh, B. Stix, T. Rath, T. Kähne, J. Dierkes, A. Roessner, F.W. Albert, ALys amyloidosis caused by compound heterozygosity in exon 2 (Thr70Asn) and exon 4 (Trp112Arg) of the lysozyme gene, Hum. Mutat. (2006), https://doi.org/10.1002/humu.9393.
[11] P.J. Artymiuk, C.C.F. Blake, Refinement of human lysozyme at 1.5 Å resolution analysis of non-bonded and hydrogen-bond interactions, J. Mol. Biol. (1981), https://doi.org/10.1016/0022-2836(81)90125-X.
[12] A. Moura, P. Nocerino, J.A. Gilbertson, N.B. Rendell, P.P. Mangione, G. Verona, D. Rowczenio, J.D. Gillmore, G.W. Taylor, V. Bellotti, D. Canetti, Lysozyme amyloid: evidence for the W64R variant by proteomics in the absence of the wild type protein, Amyloid (2020), https://doi.org/10.1080/13506129.2020.1720637.
[13] M. Dumoulin, R.J.K. Johnson, V. Bellotti, C.M. Dobson, Human lysozyme, in: Protein Misfolding, Aggregation, Conform. Dis, 2007, https://doi.org/10.1007/978-0-387-36534-3_14.
[14] D. Canet, A.M. Last, P. Tito, M. Sunde, A. Spencer, D.B. Archer, C. Redfield, C. V. Robinson, C.M. Dobson, Local cooperativity in the unfolding of an amyloidogenic variant of human lysozyme, Nat. Struct. Biol. (2002), https://doi.org/10.1038/nsb768.
[15] M. Dumoulin, A.M. Last, A. Desmyter, K. Decanniere, D. Canet, G. Larsson, A. Spencer, D.B. Archer, J. Sasse, S. Muyldermans, L. Wyns, C. Redfield, A. Matagne, C.V. Robinson, C.M. Dobson, A camelid antibody fragment inhibits the formation of amyloid fibrils by human lysozyme, Nature (2003), https://doi.org/10.1038/nature01870.
[16] M. Dumoulin, D. Canet, A.M. Last, E. Pardon, D.B. Archer, S. Muyldermans, L. Wyns, A. Matagne, C.V. Robinson, C. Redfield, C.M. Dobson, Reduced global cooperativity is a common feature underlying the amyloidogenicity of pathogenic lysozyme mutations, J. Mol. Biol. (2005), https://doi.org/10.1016/j.jmb.2004.11.020.
[17] R.J.K. Johnson, J. Christodoulou, M. Dumoulin, G.L. Caddy, M.J.C. Alcocer, G. J. Murtagh, J.R. Kumita, G. Larsson, C.V. Robinson, D.B. Archer, B. Luisi, C. M. Dobson, Rationalising lysozyme amyloidosis: insights from the structure and solution dynamics of T70N lysozyme, J. Mol. Biol. (2005), https://doi.org/10.1016/j.jmb.2005.07.040.
[18] J.R. Kumita, R.J.K. Johnson, M.J.C. Alcocer, M. Dumoulin, F. Holmqvist, M. G. McCammon, C.V. Robinson, D.B. Archer, C.M. Dobson, Impact of the native-state stability of human lysozyme variants on protein secretion by *Pichia pastoris*, FEBS J (2006), https://doi.org/10.1111/j.1742-4658.2005.05099.x.
[19] C.N. Pace, Determination and analysis of urea and guanidine hydrochloride denaturation curves, Methods Enzymol. (1986), https://doi.org/10.1016/0076-6879(86)31045-0.
[20] M. Dumoulin, K. Conrath, A. Van Meirhaeghe, F. Meersman, K. Heremans, L.G. J. Frenken, S. Muyldermans, L. Wyns, A. Matagne, Single-domain antibody fragments with high conformational stability, Protein Sci. (2009), https://doi.org/10.1110/ps.34602.
[21] H. El Hajjaji, M. Dumoulin, A. Matagne, D. Colau, G. Roos, J. Messens, J.F. Collet, The zinc center influences the redox and thermodynamic properties of *Escherichia coli* thioredoxin 2, J. Mol. Biol. (2009), https://doi.org/10.1016/j.jmb.2008.11.046.
[22] W. Kabsch, XDS, Acta Crystallogr. Sect. D. 66 (2010) 125–132, https://doi.org/10.1107/S0907444909047337.
[23] K. Harata, Y. Abe, M. Muraki, Full-matrix least-squares refinement of lysozymes and analysis of anisotropic thermal motion, Proteins Struct. Funct. Genet. (1998), https://doi.org/10.1002/(SICI)1097-0134(19980215)30:3<232::AID-PROT3>3.0.CO;2-M.

[24] A.J. McCoy, R.W. Grosse-Kunstleve, P.D. Adams, M.D. Winn, L.C. Storoni, R. J. Read, Phaser crystallographic software, J. Appl. Crystallogr. (2007), https://doi.org/10.1107/S0021889807021206.
[25] P.V. Afonine, R.W. Grosse-Kunstleve, N. Echols, J.J. Headd, N.W. Moriarty, M. Mustyakimov, T.C. Terwilliger, A. Urzhumtsev, P.H. Zwart, P.D. Adams, Towards automated crystallographic structure refinement with phenix.refine, Acta Crystallogr. Sect. D Biol. Crystallogr. (2012), https://doi.org/10.1107/S0907444912001308.
[26] D.R. Booth, M. Sunde, V. Bellotti, C.V. Robinson, W.L. Hutchinson, P.E. Fraser, P. N. Hawkins, C.M. Dobson, S.E. Radford, C.C.F. Blake, M.B. Pepys, Instability, unfolding and aggregation of human lysozyme variants underlying amyloid fibrillogenesis, Nature (1997), https://doi.org/10.1038/385787a0.
[27] P.D.J. Moens, M.K. Helms, D.M. Jameson, Detection of tryptophan to tryptophan energy transfer in proteins, Protein J. (2004), https://doi.org/10.1023/B:JOPC.0000016261.97474.2e.
[28] S.Y. Venyaminov, J.T. Yang, Determination of protein secondary structure, in: Circ. Dichroism Conform. Anal. Biomol, 1996, pp. 69–108, https://doi.org/10.1007/978-1-4757-2508-7_3.
[29] C.L. Hagan, R.J.K. Johnson, A. Dhulesia, M. Dumoulin, J. Dumont, E. De Genst, J. Christodoulou, C.V. Robinson, C.M. Dobson, J.R. Kumita, A non-natural variant of human lysozyme (I59T) mimics the in vitro behaviour of the I56T variant that is responsible for a form of familial amyloidosis, Protein Eng. Des. Sel. (2010), https://doi.org/10.1093/protein/gzq023.
[30] K. Takano, J. Funahashi, K. Yutani, The stability and folding process of amyloidogenic mutant human lysozymes, Eur. J. Biochem. (2001), https://doi.org/10.1046/j.1432-1327.2001.01863.x.
[31] G. Esposito, J. Garcia, P. Mangione, S. Giorgetti, A. Corazza, P. Viglino, F. Chiti, A. Andreola, P. Dumy, D. Booth, P.N. Hawkins, V. Bellotti, Structural and folding dynamic properties of the T70N variant of human lysozyme, J. Biol. Chem. (2003), https://doi.org/10.1074/jbc.M211000200.
[32] P. Polverino de Laureto, E. Frare, R. Gottardo, H. van Dael, A. Fontana, Partly folded states of members of the lysozyme/lactalbumin superfamily: a comparative study by circular dichroism spectroscopy and limited proteolysis, Protein Sci. (2009), https://doi.org/10.1110/ps.0205802.
[33] M. Ahn, C.L. Hagan, A. Bernardo-Gancedo, E. De Genst, F.N. Newby, J. Christodoulou, A. Dhulesia, M. Dumoulin, C.V. Robinson, C.M. Dobson, J. R. Kumita, The significance of the location of mutations for the native-state dynamics of human lysozyme, Biophys. J. (2016), https://doi.org/10.1016/j.bpj.2016.10.028.
[34] F. Chiti, C.M. Dobson, Protein misfolding, amyloid formation, and human disease: a summary of progress over the last decade, Annu. Rev. Biochem. (2017), https://doi.org/10.1146/annurev-biochem-061516-045115.
[35] M. Ahn, C.A. Waudby, A. Bernardo-Gancedo, E. De Genst, A. Dhulesia, X. Salvatella, J. Christodoulou, C.M. Dobson, J.R. Kumita, Application of lysine-specific labeling to detect transient interactions present during human lysozyme amyloid fibril formation, Sci. Rep. (2017), https://doi.org/10.1038/s41598-017-14739-5.
[36] C. Pain, J. Dumont, M. Dumoulin, Camelid single-domain antibody fragments: uses and prospects to investigate protein misfolding and aggregation, and to treat diseases associated with these phenomena, Biochimie (2015), https://doi.org/10.1016/j.biochi.2015.01.012.
[37] P.H. Chan, E. Pardon, L. Menzer, E. De Genst, J.R. Kumita, J. Christodoulou, D. Saerens, A. Brans, F. Bouillenne, D.B. Archer, C.V. Robinson, S. Muyldermans, A. Matagne, C. Redfield, L. Wyns, C.M. Dobson, M. Dumoulin, Engineering a camelid antibody fragment that binds to the active site of human lysozyme and inhibits its conversion into amyloid fibrils, Biochemistry (2008), https://doi.org/10.1021/bi8005797.